Icarus 457 (2026) 117149

Contents lists available at ScienceDirect

Icarus

journal homepage: www.elsevier.com/locate/icarus

Research Paper

An examination of the evidence for and feasibility of a molten silicate basal layer in Mars' mantle

Stuart Russell [a,b,*], Katrin Hannemann [a], Sanne Cottaar [c], Ana-Catalina Plesa [d], Christine Thomas [a,e], Doris Breuer [d]

[a] Universität Münster, Institute of Geophysics, 48149 Münster, Germany
[b] James Cook University, 1 James Cook Drive, Douglas, Queensland, 4814, Australia
[c] Bullard Laboratories, Department of Earth Sciences, University of Cambridge, CB3 0EZ, UK
[d] German Aerospace Center (DLR), Institute of Space Research, 12489 Berlin, Germany
[e] Geological Survey of Denmark and Greenland, 1350 Copenhagen, Denmark

ARTICLE INFO

Dataset link: https://doi.org/10.18715/seis.insight.xb_2016, https://doi.org/10.12686/a19, https://doi.org/10.18715/IPGP.2023.llxn7e6d, https://doi.org/10.5281/zenodo.8148831, https://doi.org/10.25928/mbx6-hr74

Keywords:
Geophysics
Planetary dynamics
Mars, interior

ABSTRACT

One of the aims of the InSight mission was to seismically constrain the size and character of Mars' core, however, seismology on Mars is challenging, involving the interpretation of low-amplitude signals with a relatively high noise level from small magnitude marsquakes on a single seismometer. Two recent papers propose a smaller core than previous studies that is overlain by a molten layer at the base of Mars' mantle. Here we suggest that the seismic observations presented in support of this conclusion can be alternatively explained by scattering in the mantle, and that a basal layer is therefore not required by the data. Furthermore, we discuss several problems for the evolution and dynamics of Mars arising from the presence of the basal layer. We suggest that other possibilities should be considered, and that significant further investigation is required to determine the structure of Mars' lowermost mantle and core.

1. Introduction

Prior to the InSight mission, estimations of Mars' core radius varied widely. Okal and Anderson (1978) suggested a core radius of half the planetary radius (1695 km), while more recently Khan et al. (2018) and Bagheri et al. (2019) suggested ranges of 1730–1840 km and 1750–1890 km, respectively. Following the deployment of InSight, observations of shear reflected (Stähler et al., 2021) and transmitted waves (Irving et al., 2023) were used to estimate the radius of the solid–fluid interface, interpreted as the core-mantle boundary (CMB), at 1830 ± 40 km and 1780–1810 km, respectively. These values imply a core with a relatively high abundance of light elements, suggested to be in contradiction with cosmochemical constraints (Steenstra and van Westrenen, 2018; Khan et al., 2022). Two more recent studies (Khan et al., 2023; Samuel et al., 2023) revise the interpretation of the solid–fluid interface. They invoke the existence of a molten silicate layer at the base of the mantle with a thickness of ~150 km, and thus the previously observed solid–fluid interface is a silicate-silicate boundary, with the true silicate–metal CMB being the fluid–fluid interface at the base of the layer. The proposed metallic core is then smaller and denser, and its composition more easily fits within the cosmochemical constraints. In support of this, both papers present the same seismological data; the primary constraint is a single seismic arrival from an impact event at 126° epicentral distance from the lander. This arrival was originally identified as a P core-diffracted (P_{diff}) phase (Horleston et al., 2022; Durán et al., 2022a), but its interpretation was revised by Khan et al. (2023) and Samuel et al. (2023) to be a P-wave that interacts with the molten silicate layer. In the following sections, we highlight various concerns about the identification and revision of this phase, present an alternative explanation for the data that does not require a basal layer to the mantle, and discuss other potential issues that could arise if this layer were to exist.

2. Seismology - Modelling

Samuel et al. (2023) and Khan et al. (2023) both reach similar conclusions regarding the basal layer, but the seismic interpretations differ between the two studies. Samuel et al. (2023) suggest that the phase diffracts along the top of a layer, with a reverberation within it, which they call $Pb_{diff}PcP$. In contrast, Khan et al. (2023) interpret the phase to diffract along the base of the layer, which they call P_{diff}^{CMB} to differentiate from the earlier arriving P_{diff}^{LSL} that diffracts along the

* Corresponding author.
E-mail address: stuart.russell@jcu.edu.au (S. Russell).

https://doi.org/10.1016/j.icarus.2026.117149
Received 8 September 2025; Received in revised form 28 April 2026; Accepted 30 April 2026
Available online 13 May 2026

layer top. They also interpret a phase named P_{diff} ^LSL P_{diff} in the data, which is interpreted to have an additional bounce within the layer. The ray paths that interact with the layer as proposed by the two papers are shown in Fig. 1a and b, and examples of other relevant ray paths are shown in Supplementary Figure S1. The ray path suggested by Khan et al. (2023) for P_{diff}^{CMB} is non-physical as, according to Snell's law, a P-wave descending through the layer will transmit and reflect at the core interface, as proposed by Samuel et al. (2023), rather than diffract along the interface.

Both papers use the ray paths as part of a body wave travel time inversion in order to deduce the seismic properties of the layer, where the forward problem is the calculation of travel times based on the ray path. It is therefore important to ascertain the sensitivity of the path as this underpins the inversion results. Both papers use the software TauP (Crotwell et al., 1999) to compute ray-theoretical paths for potentially interpreted phases, however, diffracted phases do not adhere to ray-theoretical principles. Nevertheless, diffraction is a well-studied phenomenon and TauP handles diffraction with hard-coded exceptions. When applying TauP to complex velocity models or non-standard diffracted phases, one must be careful as there can be unintended consequences and the output of non-physical raypaths. Furthermore, studies on Earth have highlighted the need to avoid ray-theoretical approaches in relation to P_{diff} observations and to instead use sensitivity kernels (e.g. Kárason and van der Hilst, 2001; Hosseini and Sigloch, 2015), which relate a synthetic seismic arrival to its spatial sensitivity to the model parameters. Sensitivity kernels can be calculated from AxiSEM synthetics (Nissen-Meyer et al., 2014), which both papers present, and doing so eliminates any speculation about the nature of the synthetic arrivals.

We use AxiSEM to calculate 2 s synthetics for a model with a velocity inversion between the base of the molten layer and the core (similar to BML Supplementary Layer 2 of Samuel et al. (2023)); the velocity inversion amplifies the phase that reflects off the base and exists in models from both papers. We calculate P-velocity sensitivity kernels using MC Kernel (Stähler et al., 2016) for a 2 s database filtered with a 2–8 s zero-phase bandpass filter for both the Pb_{diff} (or P_{diff}^{LSL}) phase and the later arriving phase (Fig. 1). The kernels clearly display the paths of both phases. The Pb_{diff} (or P_{diff}^{LSL}) propagates along the top of the layer and, as expected, has no sensitivity to the layer itself (Fig. 1e), while the second phase is consistent with the ray path interpreted by Samuel et al. (2023): a diffracted phase along the top of the layer with broad sensitivity below the diffraction due to reverberation within the layer (Fig. 1f). The Khan et al. (2023) ray path would be expected to have concentrated sensitivity at the base of the layer with a clear pair of up- and down-going legs; this demonstrates that the Khan et al. (2023) ray path is not the phase in the synthetics. We note that the models of Samuel et al. (2023) include a thin partial molten layer at the top of the layer creating a gradual transition in velocity, a feature absent in the sharp-topped layers of Khan et al. (2023); this difference does not significantly affect the sensitivity kernels (Supplementary Figure S2).

3. Seismology - Data

Next, we consider whether the energy in the data corresponds to $Pb_{diff}PcP$, as exists in the synthetics. One issue with $Pb_{diff}PcP$ is that it relies on the constructive interference of infinite possible raypaths that reverberate within the layer. In synthetics, this occurs perfectly because the layer lacks topography, both at its top and at the CMB. However, Mars' mantle is convecting and topography is expected, the most likely effect of which would be to reduce the amplitude of $Pb_{diff}PcP$ compared to Pb_{diff}, as the reverberations within the layer decorrelate. With or without topography, for most likely velocity models, the phase with a reflection at the CMB, $Pb_{diff}PcP$, would be expected to have a lower amplitude than Pb_{diff}. Therefore, it is not clear why $Pb_{diff}PcP$ is interpreted, but Pb_{diff} is absent in Samuel et al. (2023). Khan et al. (2023) does interpret an earlier arrival that could be Pb_{diff}, as well as a later phase that would have bounced again within the layer. Interestingly, the amplitude of each later interpreted phase is stronger than that of the earlier phase, which is not expected with additional reflections in the layer.

In Fig. 2 we present further analysis of the data itself. Filtered seismograms are shown in Panel a, clearly illustrating the low-amplitude signals interpreted by both papers. Panel b shows the time-dependent normalized azimuthal density (polarization), which represents a modified version of Figure S10b of Khan et al. (2023). To ensure that we only analyse the largest amplitude signals, we restrict the presented results to those time–frequency points for which the overall amplitude is larger than the 5th percentile of all amplitude estimates for the whole time window. Furthermore as P-waves are expected to have low ellipticity we restrict to points where the ellipticity is smaller than 0.4. Panel c is the same but for 0.4–0.8 Hz, being close to the frequency bands used by Samuel et al. (2023). In both plots there is energy arriving from the approximate back-azimuth to the event (34°), but this is generally unstable with orthogonal energy also present.

Panel d shows the spectral content of the vertical component seismogram calculated from the envelope of band pass filtered data, for which we use second-order, zero-phase filters with half-octave width every tenth of an octave. In order to visually enhance the weak energy arrivals, we calculate the difference between the envelope and the median of the envelope for each frequency band. In the marked time windows before PP, weak arrivals with narrow frequency content can be identified, but there is also a gradual increase in energy observed with time. The gradual increase in energy up to PP is especially pronounced in Panel e, where the power spectral density (PSD) is presented for three different frequency bands for all components. All components and frequency bands show a slow increase in amplitude over time, with the only significant jump in energy being PP in the 0.4–0.8 Hz band.

Following the MQS P_{diff} pick at ~17:59 there is a slight change in character of the polarization with an increase of the orthogonal energy, possibly indicating the presence of S-wave energy. This coincides with an increase in the spectral content between 0.1–1.0 Hz, but there are no notable bumps in the PSD. These observations are inconsistent with discrete seismic arrivals and, as we shall show in the next section, suggests the arrival of a diffuse and scattered wavefield.

4. Seismology - Scattering

Seismic scattering is caused by short-wavelength variations in elastic properties in the lithosphere and mantle, which scatter seismic energy in different directions, leading to significant complexity in seismograms (for an overview of seismic scattering see Shearer, 2015). Scattered energy can arrive either before or after a main seismic phase, depending on the geometry, and manifests itself as broadly two types, either as discrete and coherent seismic arrivals or as an elongated train of incoherent energy. Both types have their own causal mechanisms and can often occur together (e.g. Ma and Thomas, 2020). Scattering is also frequency dependent (Aki and Chouet, 1975; Ritter et al., 1997; Shearer, 2015) and leads to significant P-energy on the transverse component (Gupta and Blandford, 1983; Cessaro and Butler, 1987), which is otherwise expected to be minimal around P-waves.

For the InSight data from S1000a there are two classes of scattering that are relevant that have been studied on Earth. Firstly, there is post-P_{diff} scattering (e.g. Bataille and Lund, 1996; Jagt et al., 2024; Zhang et al., 2024) caused predominantly by seismic velocity variations close to the CMB (Bataille et al., 1990; Bataille and Lund, 1996; Zhang et al., 2024). If P_{diff} does occur in the S1000a data prior to PP, then subsequent arrivals due to scattering are expected even in the absence of a mantle basal layer; it is even possible for scattering to mimic P_{diff} itself (Zhang et al., 2024) and so identifying P_{diff} and associated phases requires a great deal of care. Secondly, in the minutes preceding PP there is pre-cursory scattering (e.g. Shearer, 1990; Rost et al., 2008; Bentham et al., 2017; Yuan et al., 2023). Pre-PP scattering is highly

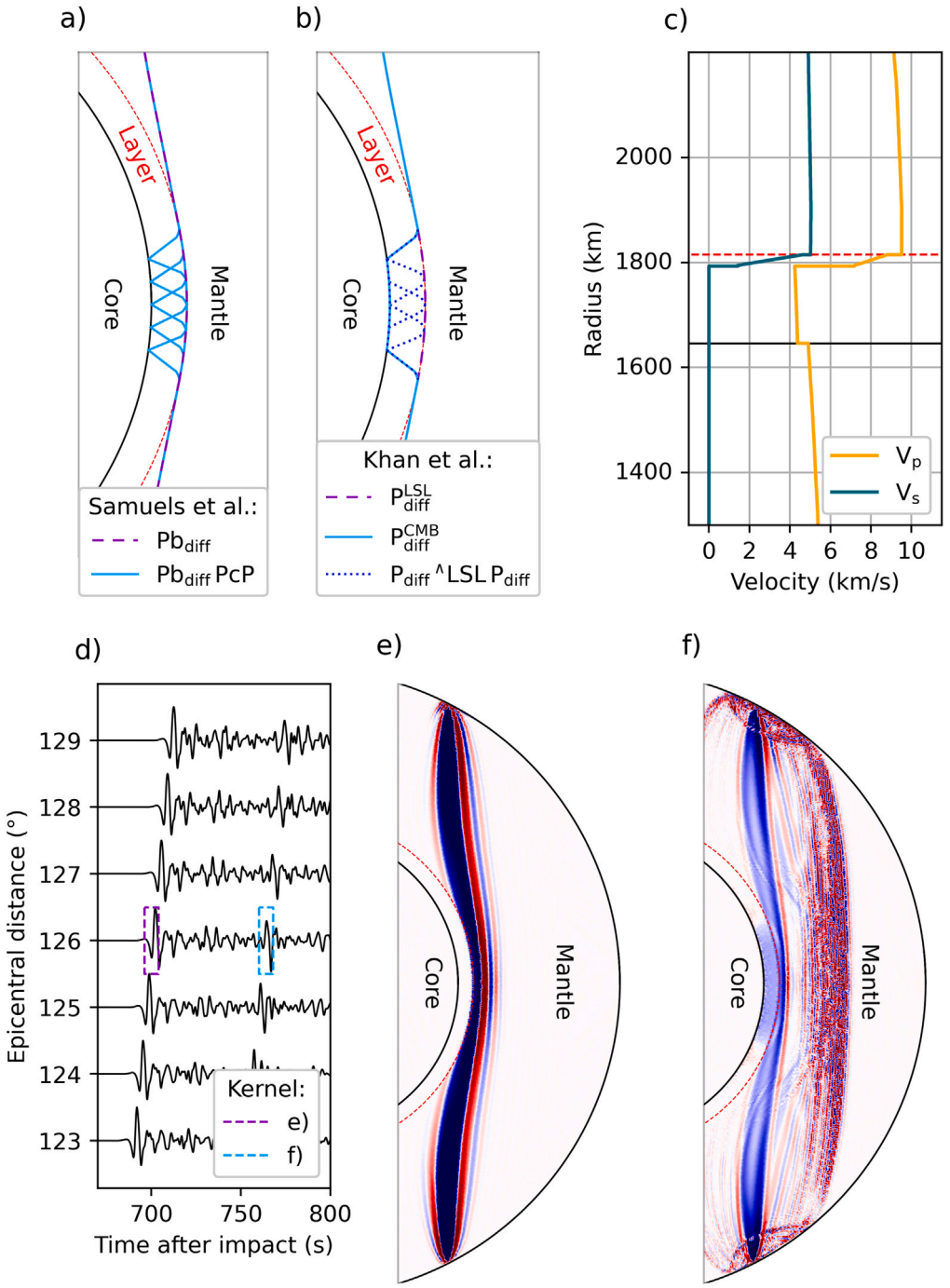

Fig. 1. (a) Ray paths for phases from Samuel et al. (2023), colours correspond to the boxes in Panel d. The black line marks the CMB and the dashed red line marks the top of the layer. (b) As for Panel a but for phases from Khan et al. (2023). (c) P- and S- velocity profiles for the model used to calculate the synthetics and kernels. (d) Vertical component synthetic waveforms band-pass filtered 2.0–8.0 s. (e) Delay-time sensitivity kernel for the purple box in Panel d. Darker colours depict greater sensitivity — the colour scale is truncated in order to emphasize sensitivity in the lower mantle. (f) As for Panel e, but for the second phase corresponding to the light blue box in Panel d. (For interpretation of the references to color in this figure legend, the reader is referred to the web version of this article.)

complex and has a range of causes; there are both discrete arrivals and incoherent energy associated with reflections from mantle discontinuities (e.g. Shearer, 1990; Deuss, 2009), mid-mantle scatterers (e.g. Rost et al., 2006; Bentham et al., 2017; Kaneshima, 2016; Yuan et al., 2023), and crustal structure (e.g. King et al., 1975).

To demonstrate how this scattering appears in seismograms, we show P_{diff} and PP waveforms for three earthquakes recorded at the Black Forest Observatory (BFO) in south-western Germany in Fig. 3. Here we only show the waveforms, but the same analysis as shown for the Mars data in Fig. 2 is shown for all three events in Supplementary Section S3. The first set of waveforms (27. July 2015) show relatively clean seismograms that have clear P_{diff} and PP on the Z component with no other notable arrivals of P-energy until the inner core reflected phase, PKiKP. Although PP is somewhat emergent, these seismograms show what these phases should look like in a best-case scenario with minimal scattering. The second set of waveforms (08. August 1993)

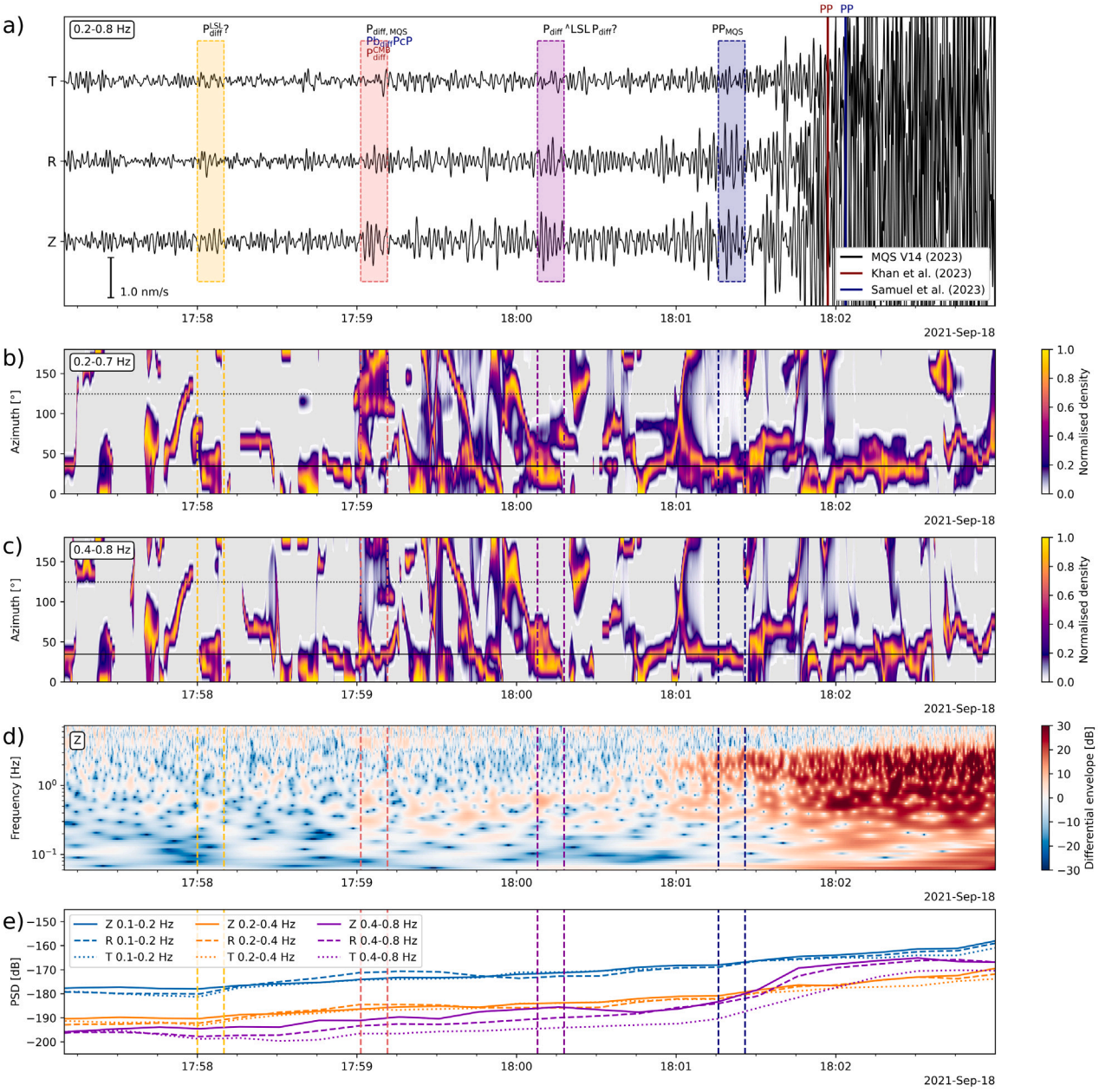

Fig. 2. (a) Three-component (TRZ) velocity seismograms, fourth-order band pass filtered 0.2–0.8 Hz for event S1000a. Four 10 s long time windows are highlighted: the yellow box contains P^{LSL}_{diff}; the red box contains the Marsquake Service (MQS) P_{diff} / P^{CMB}_{diff} / $Pb_{diff}PcP$; the purple box contains P_{diff} ^LSL P_{diff}; and the blue box contains PP (Ceylan and Giardini alignment from InSight Marsquake Service (2023)). The red and blue lines mark the PP arrival times used by Khan et al. (2023) and Samuel et al. (2023), respectively. (b) Temporal change in normalized azimuthal density in the 0.2–0.7 Hz frequency band resulting from time–frequency-polarization analysis (Sollberger, 2023), performed in five-period-long time windows. Only time–frequency points with an amplitude above the 5th percentile of all amplitudes in the time–frequency domain and an ellipticity below 0.4 are shown; grey colours are below these thresholds. Black horizontal lines indicate the expected back-azimuth to impact (34°, solid) and perpendicular to this (124°, dotted). (c) As for b, but for 0.4–0.8 Hz. (d) Differential envelopes of the Z component for half-octave wide second-order zero-phase band pass filters every tenth of an octave starting at 0.05 Hz. (e) 95th percentile of PSD for three different octave-wide frequency bands between 0.1 Hz and 0.8 Hz calculated for one-minute time windows every 15 s for ZRT components. (For interpretation of the references to color in this figure legend, the reader is referred to the web version of this article.)

show unambiguous scattering that remains above the noise from P_{diff} to PP — all of this energy can be safely attributed to scattering, including potential reflections from mantle discontinuities. The third set of waveforms (14. July 2019) are more ambiguous. P_{diff} itself is not readily visible, but there is an increase in energy after its expected arrival up to PP. These waveforms are remarkably similar to the S1000a waveforms in character and, as demonstrated in Supplementary Section S3, contain notable scattered energy. These waveforms demonstrate how complex post-P_{diff} and pre-PP scattering can be, and that seismic arrivals between these two phases must be interpreted with care, even on Earth where we know that there is not a presently molten basal mantle layer.

While on Earth these scatterers largely emerge and are studied as post-P_{diff} and pre-PP, related to heterogeneity in the lowermost and the upper mantle, respectively, the time between P_{diff} and PP can also be thought of as a near-continuous ensemble of scattering originating from a variety of locations within a planet's interior. Supplementary Figure S3 shows kernels for a series of narrow time windows within

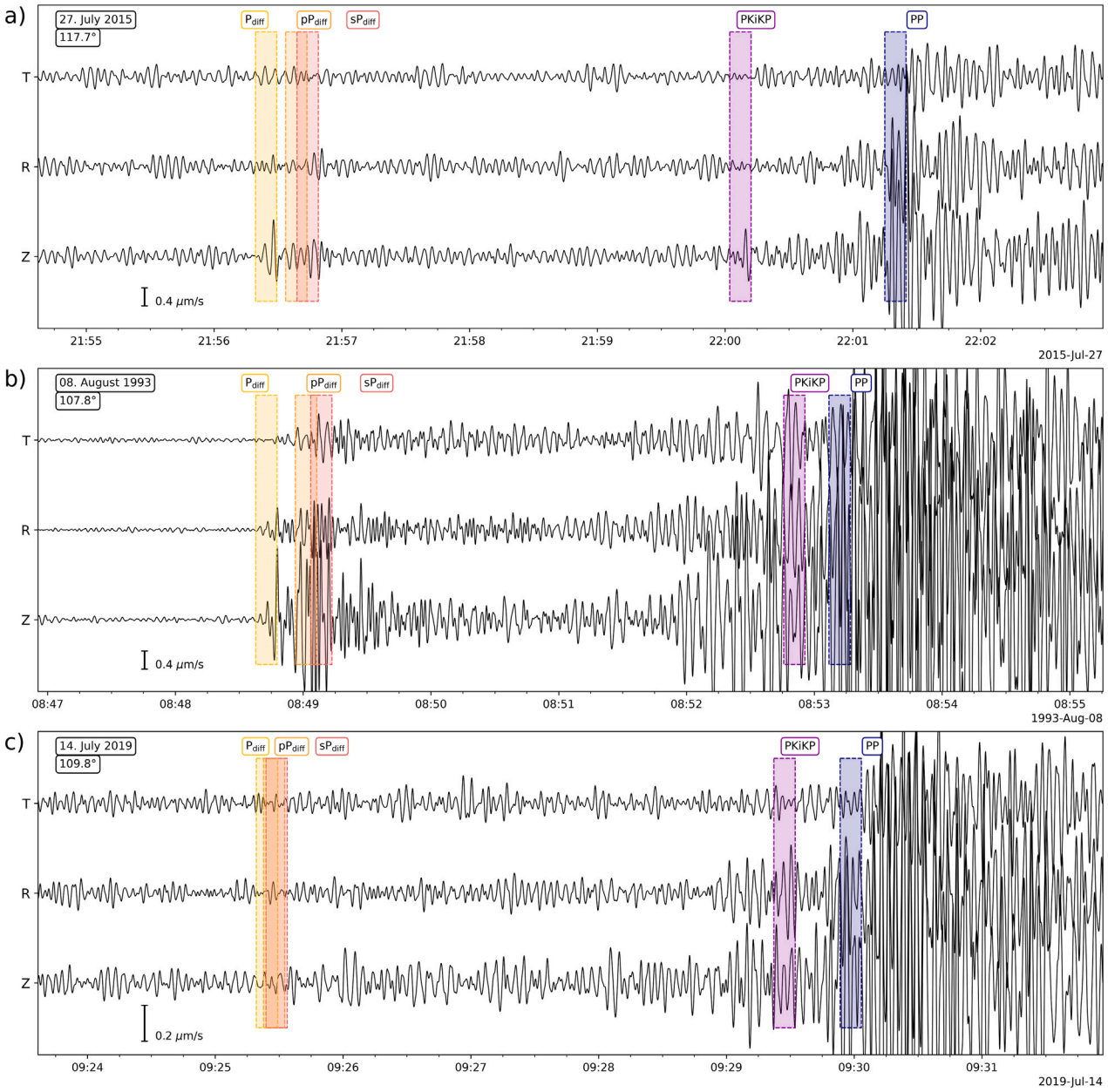

Fig. 3. Three-component velocity seismograms recorded at BFO for three different earthquakes (see Supplementary Table S1 for earthquake details) — the date and epicentral distances are given in the top left of each plot. Waveforms are filtered from 0.2–0.8 Hz using a second order, zero-phase filter, the same frequency band as used in Fig. 2a. Arrival times are ray-theoretical and calculated for the ak135 Earth model (Kennett et al., 1995). The vertical scale is marked in the bottom left of each plot.

the relevant time frame to show how the locus of points for in-plane scatterers evolves. The general trend is for the scatterers to become shallower with time, however, all of the time windows have significant sensitivity to the upper mantle and crust, which is known to cause scattering on Mars (Banerdt et al., 2020; Lognonné et al., 2020; van Driel et al., 2021; Karakostas et al., 2021; Menina et al., 2023). Scattering from the crust would also be most energetic and prolonged for shallow seismic sources (Shearer and Earle, 2004), such as the impact event of S1000a. Furthermore, InSight data has shown Mars' mantle to be highly heterogeneous and scattering throughout (Charalambous et al., 2025), which would cause prolonged scattering between P_{diff} and PP. Another point is that the phases picked by Samuel et al. (2023) and Khan et al. (2023) (Fig. 1f) are approximately co-incident with underside reflections from proposed mantle discontinuities independently proposed based on Insight data (see Supplementary Table S2; Deng and Levander, 2020; Huang et al., 2022; Deng and Levander, 2023; Durán et al., 2025). It is important to note, that while the kernels show potential locations that could cause in-plane scatterings, the significant energy on the transverse component for the Martian data suggests out-of-plane energy is also present.

While there is certainly energy from the direction of marsquake S1000a, its characteristics are comparable to scattering on Earth and scattering is known to be prevalent from heterogeneity in the Martian crust and mantle, as it is on Earth. The narrow frequency character of the S1000a arrivals and the gradual increase in energy before the PP wave for all three components, including the transverse, indicates that these phases are part of a diffuse scattered wavefield with in- and out-of-plane energy. While it is possible that P_{diff} and other coherent seismic phases may occur in the time window, coherent energy is also possible in such scattered wavefields and occurs on Earth in the absence

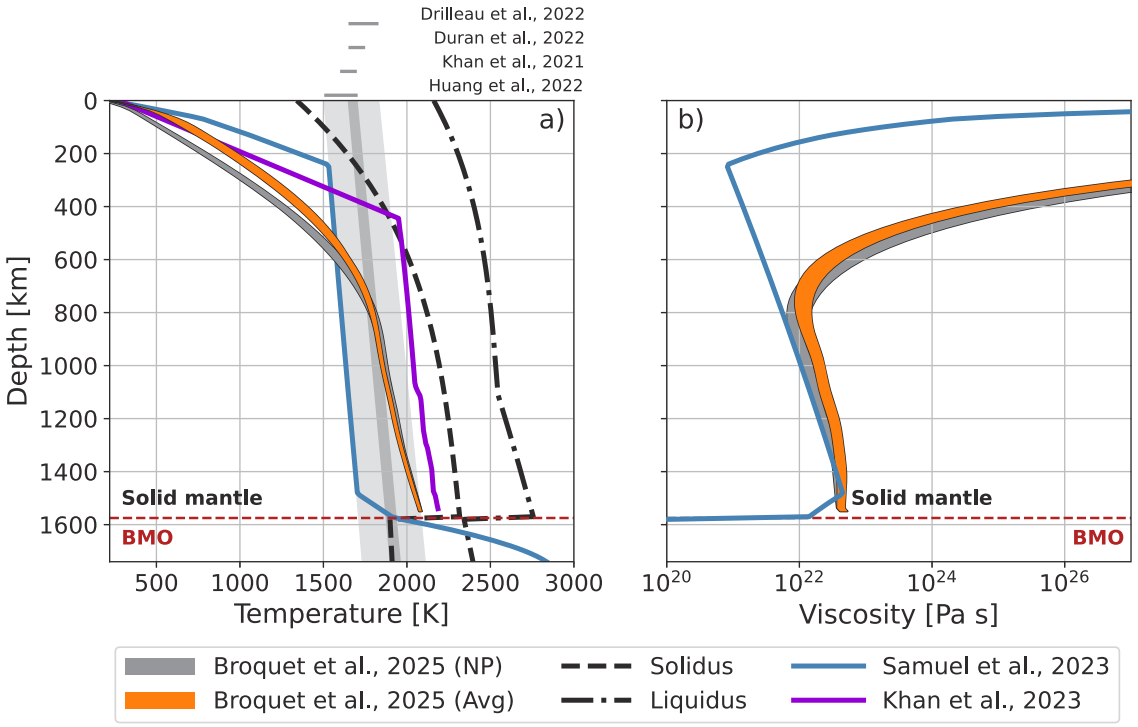

Fig. 4. (a) Temperature profiles from Samuel et al. (2023) and Khan et al. (2023) compared to previous estimates derived from seismic measurements of InSight and to the preferred models from Broquet et al. (2025), both the average temperature profile (Avg) and that beneath the northern polar cap (NP). For the Khan et al. (2023) profile we use Model 10, which is representative of the suite of models presented, and Khan et al. (2023) only provide the temperature in the solid mantle. The dark grey band shows only the adiabatic temperature profiles that are consistent with all previous studies simultaneously (i.e., Huang et al., 2022; Khan et al., 2021; Drilleau et al., 2022; Durán et al., 2022a), while the light grey band shows the largest possible temperature range based on the lowest estimates from Huang et al. (2022) (1605 ± 100 K) and the highest values from Drilleau et al. (2022) (1740 ± 90 K). For comparison we also plot the solidus and liquidus temperature and note that many temperature profiles presented by Khan et al. (2023) exceed the melting temperature suggesting a global partial melt layer in the shallow Martian mantle today. (b) Viscosity profile from Samuel et al. (2023) calculated with $\eta_0 = 5 * 10^{20}$ Pa; $E = 110$ kJ/mol; $V = 4.4$ cm^3/mol and from Broquet et al. (2025), both the average viscosity profile (Avg) and that beneath the northern polar cap (NP). We note that Khan et al. (2023) do not provide viscosity profiles or parameters to calculate them.

of a basal mantle layer. We do not believe that these phases can be safely reinterpreted as phases originating from a molten basal layer to Mars' Mantle.

5. Geodynamics

In addition to the concerns regarding the seismic evidence, a present-day molten layer at the base of Mars' mantle is challenging to reconcile with Mars' thermal evolution, specifically the dynamo history, the distribution of heat producing elements (HPEs), and the observed low deflection observed beneath the northern polar cap. This layer is suggested to form early in the evolution as a consequence of magma ocean solidification and overturn of late stage cumulates rich in iron and HPEs (Elkins-Tanton et al., 2003). Once at the base of the mantle, these hot, dense cumulates will give rise to a so-called basal magma ocean that is suggested to survive until present day (Khan et al., 2023; Samuel et al., 2023). However, such a molten layer prevents efficient core cooling and therefore the generation of a core-dynamo (Hsieh et al., 2024), at odds with observational evidence that indicates an active dynamo until at least 3.7 Ga (Mittelholz et al., 2020). While alternative scenarios for the generation of a dynamo on Mars have been proposed by Samuel et al. (2023) (e.g., enhanced heat flux due to magma ocean cumulate overturn, effects of giant impacts, core instabilities excited through tidal interaction with ancient satellites), these scenarios produce too short-lived dynamos (Elkins-Tanton et al., 2005), may actually suppress the dynamo (Arkani-Hamed and Olson, 2010), or are not compatible with a suggested active dynamo younger than the formation of the giants impacts ~4 Ga (Arkani-Hamed, 2009).

The Martian magnetic field could have been generated within the iron-rich molten layer at the base of the mantle (Helffrich, 2017), however vigorous convection, which is necessary for dynamo generation would result in efficient heat loss and crystallization. To keep this layer molten, Samuel et al. (2021) argue for HPE enrichment and stable stratification. The latter is due to its iron enrichment with depth (Samuel et al., 2021), however in this case the layer would not convect and therefore not generate a dynamo.

Another issue concerns the distribution of HPEs. Gamma-ray surface measurements indicate a strong crustal enrichment in HPEs (>50% bulk abundance, Hahn et al., 2011). While these measurements are only sensitive to the uppermost few centimetres, no anomalies associated with large impact basins, which would sample a poorly enriched lower crust, have been recorded, suggesting that the surface abundance is likely representative of deeper crustal layers as well (Taylor et al., 2006). If most of the HPEs have fractionated into and remain trapped within the basal mantle layer to keep it molten (Samuel et al., 2021), then the observed crustal enrichment is difficult to explain.

Although the papers by Khan et al. (2023) and Samuel et al. (2023) reach a similar conclusion regarding a molten silicate layer at the base of the Martian mantle, there are differences in the thermal state of the solid mantle between the papers (Fig. 4a). The solid mantle in the study of Samuel et al. (2023) lies at the lower bound of the temperature range suggested by the previous seismic study of Huang et al. (2022). The temperature profiles shown in Samuel et al. (2023, 2021), satisfy the observation of the global quality factor $Q_2 = 95 \pm 10$ derived from the main tidal period of Phobos (Pou et al., 2022). However, the profile for the basal magma ocean case shows thin thermal and consequently elastic lithospheres (Fig. 4b). The thermal lithosphere is

too thin to explain the electromagnetic induction data from Mars Global Surveyor (Drilleau et al., 2026). Moreover, for the best-fit thermal profile of Samuel et al. (2023), the elastic lithosphere thickness – not to be confused with the generally thicker thermal lithosphere – is less than 200 km, which is too thin to explain the low deflection observed underneath the north polar cap today (Broquet et al., 2025) (see also Supplementary Section S5). This still applies when taking into account that Samuel et al. (2023) calculated a mean viscosity profile and that the viscosity under the north pole could be higher due to lateral temperature and viscosity variations. Even when using a 3D model of thermal evolution accounting for the thermal insulation effect of a spatially variable crustal thickness – derived from gravity and topography data – the thermal and viscosity profiles consistent with the current deflection beneath the north pole resemble the average profiles (Broquet et al., 2025, and Fig. 4). This implies that no significant variation is expected between the averaged profiles beneath the north polar cap and the average profiles of the entire planet. 2D thermochemical evolution models showing a present-day magma ocean (Cheng et al., 2025) also point to too thin average lithospheres — also inconsistent with observations of the low deflection of the north polar cap (Broquet et al., 2025) and electrical conductivity data (Drilleau et al., 2026).

The model by Samuel et al. (2023) without a basal magma ocean is consistent with Q and a thick elastic lithosphere, as already demonstrated by Plesa et al. (2018). The mantle temperatures obtained by Khan et al. (2023), on the other hand, are at the upper end of the highest temperatures suggested by previous models (Drilleau et al., 2022), with values exceeding the melting temperature. This would lead to the presence of a global partially molten layer in the upper part of the mantle, which is inconsistent with the absence of widespread volcanic activity on Mars in recent times. In addition, the Khan et al. (2023) temperature profiles also strongly suggest that mantle viscosities are too low, assuming typical viscosity parameters, which is also not consistent with the observation of low surface deformation. Moreover, the studies by Khan et al. (2023) and Samuel et al. (2023) lie outside the range of temperatures that is consistent with all previous studies that used InSight seismic data to constrain the thermal state of the Martian interior (Huang et al., 2022; Drilleau et al., 2022; Durán et al., 2022b; Khan et al., 2021).

6. Summary

We do not dispute that there are arrivals of seismic energy preceding PP, however, we have outlined a number of concerns regarding the reinterpretation that these provide evidence for a molten basal layer to Mars' mantle. We show that the waves preceding the surface reflection, PP, exist within an emergent wavefield containing multi-directional narrow-frequency-band energy, and thus propose P_{diff} or subsequent scattering as a simpler alternative explanation. Very similar seismic arrivals are observed on Earth and it is our view that a basal layer to Mars' mantle is not required by the data. We have also discussed difficulties in reconciling a basal mantle layer with the Martian magnetic field history and the HPE distribution, as well as highlighting inconsistencies with the inferred temperature and corresponding viscosity profiles for Martian mantles with a molten layer. Whether the interpretation presented in these two studies reflects the interior of Mars requires careful further investigation. We do not consider the evidence thus far to be conclusive and we caution against treating a molten mantle basal layer on Mars as proven.

CRediT authorship contribution statement

Stuart Russell: Writing – review & editing, Writing – original draft, Visualization, Validation, Software, Methodology, Investigation, Formal analysis, Data curation, Conceptualization. **Katrin Hannemann:** Writing – review & editing, Writing – original draft, Visualization, Validation, Software, Methodology, Investigation, Formal analysis, Data curation, Conceptualization. **Sanne Cottaar:** Writing – review & editing, Writing – original draft, Visualization, Validation, Methodology, Investigation, Formal analysis, Conceptualization, Data curation, Software. **Ana-Catalina Plesa:** Writing – review & editing, Writing – original draft, Visualization, Validation, Methodology, Investigation, Formal analysis, Conceptualization, Data curation, Software. **Christine Thomas:** Writing – review & editing, Writing – original draft, Visualization, Validation, Methodology, Investigation, Formal analysis, Conceptualization, Data curation, Software. **Doris Breuer:** Writing – review & editing, Writing – original draft, Visualization, Validation, Methodology, Investigation, Formal analysis, Conceptualization, Data curation, Software.

Declaration of competing interest

The authors declare that they have no known competing financial interests or personal relationships that could have appeared to influence the work reported in this paper.

Acknowledgments

We thank Alessandro Morbidelli as editor and one anonymous reviewer. We would also like to thank Amir Khan for his constructive feedback during the preparation of this piece. Many thanks to Adrien Broquet, who provided us with calculations of the deformation of the surface beneath the north polar cap using his viscoelastic model. S.C. has received funding from the European Research Council (ERC) under the European Union's Horizon 2020 research and innovation programme (grant agreement No. 804071 -ZoomDeep) and the Natural Environment Research Council [NERC grant reference number NE/V018213/1]. S.R acknowledges funding from the Deutsche Forschungsgemeinschaft (DFG), grant number TH1530/16-3. The synthetic modelling was performed on the computing cluster PALMA II of Universität Münster, subsidized by the DFG (INST 211/667-1) and the Cambridge Service for Data Driven Discovery (CSD3) operated by the University of Cambridge Research Computing Service (www.csd3.cam.ac.uk), provided by Dell EMC and Intel using Tier-2 funding from the Engineering and Physical Sciences Research Council (capital grant EP/T022159/1), and DiRAC funding from the Science and Technology Facilities Council (www.dirac.ac.uk).

Appendix A. Supplementary data

Supplementary material related to this article can be found online at https://doi.org/10.1016/j.icarus.2026.117149.

Data availability

Raw seismic data for InSight can be downloaded from the Incorporated Research Institutions for Seismology Data Management Center (IRIS DMC) https://doi.org/10.18715/seis.insight.xb_2016. The Marsquake Service catalogue is available at https://doi.org/10.12686/a19. The seismic velocity and temperature profiles from Khan et al. (2023) are available at: https://doi.org/10.18715/IPGP.2023.llxn7e6d, and the data from Samuel et al. (2023) are available at: https://doi.org/10.5281/zenodo.8148831. Seismic data for BFO, as well the data for other stations used to calculate the vespagrams shown in the Supplementary Section S3 can be downloaded from the Federal Institute for Geosciences and Natural Resources (BGR, Germany): https://doi.org/10.25928/mbx6-hr74.

References

Aki, K., Chouet, B., 1975. Origin of coda waves: source, attenuation, and scattering effects. J. Geophys. Res. 80 (23), 3322–3342.

Arkani-Hamed, J., 2009. Did tidal deformation power the core dynamo of Mars? Icarus 201 (1), 31–43.

Arkani-Hamed, J., Olson, P., 2010. Giant impacts, core stratification, and failure of the martian dynamo. J. Geophys. Res.: Planets 115 (E7).

Bagheri, A., Khan, A., Al-Attar, D., Crawford, O., Giardini, D., 2019. Tidal response of Mars constrained from laboratory-based viscoelastic dissipation models and geophysical data. J. Geophys. Res.: Planets 124 (11), 2703–2727.

Banerdt, W.B., Smrekar, S.E., Banfield, D., Giardini, D., Golombek, M., Johnson, C.L., Lognonné, P., Spiga, A., Spohn, T., Perrin, C., et al., 2020. Initial results from the InSight mission on Mars. Nat. Geosci. 13 (3), 183–189.

Bataille, K., Lund, F., 1996. Strong scattering of short-period seismic waves by the core-mantle boundary and the P-diffracted wave. Geophys. Res. Lett. 23 (18), 2413–2416.

Bataille, K., Wu, R., Flatte, S., 1990. Inhomogeneities near the core-mantle boundary evidenced from scattered waves: A review. Pure Appl. Geophys. 132 (1), 151–173.

Bentham, H., Rost, S., Thorne, M., 2017. Fine-scale structure of the mid-mantle characterised by global stacks of PP precursors. Earth Planet. Sci. Lett. 472, 164–173.

Broquet, A., Plesa, A.-C., Klemann, V., Root, B., Genova, A., Wieczorek, M., Knapmeyer, M., Andrews-Hanna, J., Breuer, D., 2025. Glacial isostatic adjustment reveals Mars's interior viscosity structure. Nature 639 (8053), 109–113.

Cessaro, R., Butler, R., 1987. Observations of transverse energy for P waves recorded on a deep-ocean borehole seismometer located in the northwest Pacific. Bull. Seismol. Soc. Am. 77 (6), 2163–2180.

Charalambous, C., Pike, W.T., Kim, D., Samuel, H., Fernando, B., Bill, C., Lognonné, P., Banerdt, W.B., 2025. Seismic evidence for a highly heterogeneous martian mantle. Science 389 (6763), 899–903.

Cheng, K.W., Ballmer, M.D., Tackley, P.J., Khan, A., 2025. The impact of a long-lived basal magma ocean on the thermochemical evolution of Mars. J. Geophys. Res.: Planets 130 (11), e2025JE009213.

Crotwell, H.P., Owens, T.J., Ritsema, J., et al., 1999. The TauP toolkit: Flexible seismic travel-time and ray-path utilities. Seismol. Res. Lett. 70, 154–160.

Deng, S., Levander, A., 2020. Autocorrelation reflectivity of Mars. Geophys. Res. Lett. 47 (16), e2020GL089630.

Deng, S., Levander, A., 2023. Seismic autocorrelation analysis of deep Mars. Geophys. Res. Lett. 50 (24), e2023GL105046.

Deuss, A., 2009. Global observations of mantle discontinuities using SS and PP precursors. Surv. Geophys. 30 (4), 301–326.

Drilleau, M., Samuel, H., Garcia, R.F., Rivoldini, A., Perrin, C., Michaut, C., Wieczorek, M., Tauzin, B., Connolly, J.A., Meyer, P., et al., 2022. Marsquake locations and 1-D seismic models for Mars from Insight data. J. Geophys. Res.: Planets 127 (9), e2021JE007067.

Drilleau, M., Samuel, H., Verhoeven, O., Rivoldini, A., Collinet, M., Garcia, R.F., Lognonné, P., 2026. Constraining the thermochemical structure of Mars through joint inversion of multidisciplinary geophysical data. J. Geophys. Res.: Planets 131 (2), e2025JE009303.

Durán, C., Khan, A., Ceylan, S., Charalambous, C., Kim, D., Drilleau, M., Samuel, H., Giardini, D., 2022a. Observation of a core-diffracted P-wave from a farside impact with implications for the lower-mantle structure of Mars. Geophys. Res. Lett. 49 (21), e2022GL100887.

Durán, C., Khan, A., Ceylan, S., Zenhäusern, G., Staehler, S., Clinton, J.F., Giardini, D., 2022b. Seismology on Mars: An analysis of direct, reflected, and converted seismic body waves with implications for interior structure. Phys. Earth Planet. Inter. 325, 106851.

Durán, C., Khan, A., Helffrich, G., Giardini, D., 2025. Constraints on midmantle discontinuities in Mars from analysis of InSight seismic data. Seism. Rec. 5 (2), 207–217.

Elkins-Tanton, L.T., Parmentier, E., Hess, P., 2003. Magma ocean fractional crystallization and cumulate overturn in terrestrial planets: Implications for Mars. Meteorit. Planet. Sci. 38 (12), 1753–1771.

Elkins-Tanton, L.T., Zaranek, S.E., Parmentier, E., Hess, P., 2005. Early magnetic field and magmatic activity on Mars from magma ocean cumulate overturn. Earth Planet. Sci. Lett. 236 (1–2), 1–12.

Gupta, I., Blandford, R., 1983. A mechanism for generation of short-period transverse motion from explosions. Bull. Seismol. Soc. Am. 73 (2), 571–591.

Hahn, B., McLennan, S., Klein, E., 2011. Martian surface heat production and crustal heat flow from Mars Odyssey Gamma-ray spectrometry. Geophys. Res. Lett. 38 (14).

Helffrich, G., 2017. Feasibility of a magma ocean dynamo on Mars. Prog. Earth Planet. Sci. 4 (21).

Horleston, A.C., Clinton, J.F., Ceylan, S., Giardini, D., Charalambous, C., Irving, J.C., Lognonné, P., Stähler, S.C., Zenhäusern, G., Dahmen, N.L., et al., 2022. The far side of Mars: Two distant marsquakes detected by Insight. Seism. Rec. 2 (2), 88–99.

Hosseini, K., Sigloch, K., 2015. Multifrequency measurements of core-diffracted P waves (Pdiff) for global waveform tomography. Geophys. J. Int. 203 (1), 506–521.

Hsieh, W.-P., Deschamps, F., Tsao, Y.-C., Yoshino, T., Lin, J.-F., 2024. A thermally conductive Martian core and implications for its dynamo cessation. Sci. Adv. 10 (12), eadk1087.

Huang, Q., Schmerr, N.C., King, S.D., Kim, D., Rivoldini, A., Plesa, A.-C., Samuel, H., Maguire, R.R., Karakostas, F., Lekić, V., et al., 2022. Seismic detection of a deep mantle discontinuity within Mars by Insight. Proc. Natl. Acad. Sci. 119 (42), e2204474119.

InSight Marsquake Service, 2023. Mars seismic catalogue, InSight mission; V14 2023-04-01.

Irving, J.C., Lekić, V., Durán, C., Drilleau, M., Kim, D., Rivoldini, A., Khan, A., Samuel, H., Antonangeli, D., Banerdt, W.B., et al., 2023. First observations of core-transiting seismic phases on Mars. Proc. Natl. Acad. Sci. 120 (18), e2217090120.

Jagt, L., Martin, C., Millet, F., Russell, S., Cottaar, S., 2024. P diff postcursors from the base of the Hawaiian ULVZ. Seism. Rec. 4 (3), 204–213.

Kaneshima, S., 2016. Seismic scatterers in the mid-lower mantle. Phys. Earth Planet. Inter. 257, 105–114.

Karakostas, F., Schmerr, N., Maguire, R., Huang, Q., Kim, D., Lekic, V., Margerin, L., Nunn, C., Menina, S., Kawamura, T., et al., 2021. Scattering attenuation of the Martian interior through coda-wave analysis. Bull. Seismol. Soc. Am. 111 (6), 3035–3054.

Kárason, H., van der Hilst, R.D., 2001. Tomographic imaging of the lowermost mantle with differential times of refracted and diffracted core phases (PKP, pdiff). J. Geophys. Res.: Solid Earth 106 (B4), 6569–6587.

Kennett, B.L., Engdahl, E., Buland, R., 1995. Constraints on seismic velocities in the earth from traveltimes. Geophys. J. Int. 122 (1), 108–124.

Khan, A., Ceylan, S., van Driel, M., Giardini, D., Lognonné, P., Samuel, H., Schmerr, N.C., Stähler, S.C., Durán, C., Huang, Q., et al., 2021. Upper mantle structure of Mars from InSight seismic data. Science 373 (6553), 434–438.

Khan, A., Huang, D., Durán, C., Sossi, P.A., Giardini, D., Murakami, M., 2023. Evidence for a liquid silicate layer atop the Martian core. Nature 622 (7984), 718–723.

Khan, A., Liebske, C., Rozel, A., Rivoldini, A., Nimmo, F., Connolly, J., Plesa, A.-C., Giardini, D., 2018. A geophysical perspective on the bulk composition of Mars. J. Geophys. Res.: Planets 123 (2), 575–611.

Khan, A., Sossi, P.A., Liebske, C., Rivoldini, A., Giardini, D., 2022. Geophysical and cosmochemical evidence for a volatile-rich Mars. Earth Planet. Sci. Lett. 578, 117330.

King, D., Haddon, R., Husebye, E., 1975. Precursors to PP. Phys. Earth Planet. Inter. 10 (2), 103–127.

Lognonné, P., Banerdt, W.B., Pike, W.T., Giardini, D., Christensen, U., Garcia, R.F., Kawamura, T., Kedar, S., Knapmeyer-Endrun, B., Margerin, L., et al., 2020. Constraints on the shallow elastic and anelastic structure of Mars from InSight seismic data. Nat. Geosci. 13 (3), 213–220.

Ma, X., Thomas, C., 2020. Small-scale scattering heterogeneities in the lowermost mantle from a global analysis of PKP precursors. J. Geophys. Res.: Solid Earth 125 (3), e2019JB018736.

Menina, S., Margerin, L., Kawamura, T., Heller, G., Drilleau, M., Xu, Z., Calvet, M., Garcia, R., Knapmeyer-Endrun, B., Carrasco, S., et al., 2023. Stratification of heterogeneity in the lithosphere of Mars from envelope modeling of event S1222a and near impacts: Interpretation and implications for very-high-frequency events. Geophys. Res. Lett. 50 (7), e2023GL103202.

Mittelholz, A., Johnson, C., Feinberg, J., Langlais, B., Phillips, R., 2020. Timing of the martian dynamo: New constraints for a core field 4.5 and 3.7 Ga ago. Sci. Adv. 6 (18), eaba0513.

Nissen-Meyer, T., van Driel, M., Stähler, S.C., Hosseini, K., Hempel, S., Auer, L., Colombi, A., Fournier, A., 2014. AxiSEM: broadband 3-D seismic wavefields in axisymmetric media. Solid Earth 5 (1), 425–445.

Okal, E.A., Anderson, D.L., 1978. Theoretical models for Mars and their seismic properties. Icarus 33 (3), 514–528.

Plesa, A.-C., Padovan, S., Tosi, N., Breuer, D., Grott, M., Wieczorek, M., Spohn, T., Smrekar, S., Banerdt, W., 2018. The thermal state and interior structure of Mars. Geophys. Res. Lett. 45 (22), 12–198.

Pou, L., Nimmo, F., Rivoldini, A., Khan, A., Bagheri, A., Gray, T., Samuel, H., Lognonné, P., Plesa, A.-C., Gudkova, T., et al., 2022. Tidal constraints on the Martian interior. J. Geophys. Res.: Planets 127 (11), e2022JE007291.

Ritter, J.R., Mai, P.M., Stoll, G., Fuchs, K., 1997. Scattering of teleseismic waves in the lower crust observations in the Massif Central, France. Phys. Earth Planet. Inter. 104 (1–3), 127–146.

Rost, S., Garnero, E.J., Williams, Q., 2008. Seismic array detection of subducted oceanic crust in the lower mantle. J. Geophys. Res.: Solid Earth 113 (B6).

Rost, S., Thorne, M.S., Garnero, E.J., 2006. Imaging global seismic phase arrivals by stacking array processed short-period data. Seismol. Res. Lett. 77 (6), 697–707.

Samuel, H., Ballmer, M.D., Padovan, S., Tosi, N., Rivoldini, A., Plesa, A.-C., 2021. The thermo-chemical evolution of Mars with a strongly stratified mantle. J. Geophys. Res.: Planets 126 (4), e2020JE006613.

Samuel, H., Drilleau, M., Rivoldini, A., Xu, Z., Huang, Q., Garcia, R.F., Lekić, V., Irving, J.C., Badro, J., Lognonné, P.H., et al., 2023. Geophysical evidence for an enriched molten silicate layer above Mars's core. Nature 622 (7984), 712–717.

Shearer, P.M., 1990. Seismic imaging of upper-mantle structure with new evidence for a 520-km discontinuity. Nature 344 (6262), 121–126.

Shearer, P., 2015. Deep earth structure: seismic scattering in the deep Earth. In: Treatise on Geophysics: Second Edition. pp. 759–787.
Shearer, P.M., Earle, P.S., 2004. The global short-period wavefield modelled with a Monte Carlo seismic phonon method. Geophys. J. Int. 158 (3), 1103–1117.
Sollberger, D., 2023. Solldavid/twistpy: Twistpy - first release (v0.0.1-beta).
Stähler, S.C., van Driel, M., Auer, L., Hosseini, K., Sigloch, K., Nissen-Meyer, T., 2016. MC kernel: broadband waveform sensitivity kernels for seismic tomography. In: EGU General Assembly Conference Abstracts. pp. EPSC2016–7020.
Stähler, S.C., Khan, A., Banerdt, W.B., Lognonné, P., Giardini, D., Ceylan, S., Drilleau, M., Durán, C., Garcia, R.F., Huang, Q., et al., 2021. Seismic detection of the martian core. Science 373 (6553), 443–448.
Steenstra, E.S., van Westrenen, W., 2018. A synthesis of geochemical constraints on the inventory of light elements in the core of Mars. Icarus 315, 69–78.
Taylor, G.J., Boynton, W., Brückner, J., Wänke, H., Dreibus, G., Kerry, K., Keller, J., Reedy, R., Evans, L., Starr, R., et al., 2006. Bulk composition and early differentiation of Mars. J. Geophys. Res.: Planets 111 (E3).
van Driel, M., Ceylan, S., Clinton, J.F., Giardini, D., Horleston, A., Margerin, L., Stähler, S.C., Böse, M., Charalambous, C., Kawamura, T., et al., 2021. High-frequency seismic events on Mars observed by Insight. J. Geophys. Res.: Planets 126 (2), e2020JE006670.
Yuan, Y., Sun, D., Thomas, C., 2023. A new seismic phase to detect mid-mantle scatterers. Geophys. Res. Lett. 50 (2), e2022GL100236.
Zhang, T., Sens-Schönfelder, C., Bianchi, M., Bataille, K., 2024. How P-wave scattering throughout the entire mantle mimics the high-frequency pdiff and its coda. Geophys. Res. Lett. 51 (14), e2024GL109348.